Superconductor Science and Technology

Preparation, microstructure, magnetic and transport properties of bulk textured $Bi_{1.8}Pb_{0.3}Sr_{1.9}Ca_2Cu_3O_x$ and $Bi_{1.8}Pb_{0.3}Sr_{1.9}Ca_2Cu_3O_x$+Ag ceramics

To cite this article: M I Petrov *et al* 2008 *Supercond. Sci. Technol.* **21** 105019

Supercond. Sci. Technol. **21** (2008) 105019 (10pp) doi:10.1088/0953-2048/21/10/105019

Preparation, microstructure, magnetic and transport properties of bulk textured $Bi_{1.8}Pb_{0.3}Sr_{1.9}Ca_2Cu_3O_x$ and $Bi_{1.8}Pb_{0.3}Sr_{1.9}Ca_2Cu_3O_x$ + Ag ceramics

M I Petrov[1], I L Belozerova[2], K A Shaikhutdinov[1], D A Balaev[1], A A Dubrovskii[1], S I Popkov[1], A D Vasil'ev[1] and O N Mart'yanov[3]

[1] Kirensky Institute of Physics, 660036, Krasnoyarsk, Russia
[2] Reshetnev Siberian State Aerospace University, Krasnoyarsk, Russia
[3] Boreskov Institute of Catalysis, 630090, Novosibirsk, Russia

E-mail: smp@iph.krasn.ru (M I Petrov)

Received 26 June 2008, in final form 27 June 2008
Published 21 August 2008
Online at stacks.iop.org/SUST/21/105019

Abstract

A new method of preparation of bulk textured Bi2223 ceramics and Bi2223 + Ag composites, based on room temperature pressing of foamed precursor (Bi2223, Bi2223 + Ag) in a liquid medium, is proposed. SEM and XRD data prove a high degree of texture of the bulk samples obtained. Magnetic measurements performed in directions $\boldsymbol{H} \parallel c$-axis and $\boldsymbol{H} \parallel a$–$b$-planes of Bi2223 crystallites demonstrates anisotropy of magnetization confirming the texture of the ceramics. The materials obtained possess large diamagnetic response in the direction $\boldsymbol{H} \parallel a$–$b$-planes of Bi2223 crystallites at both 77.4 and 4.2 K.

(Some figures in this article are in colour only in the electronic version)

1. Introduction

In various preparation methods of bulk textured Bi2223 ceramics, such as the powder in tube technique, sinter-forged method, etc [1–9], in most cases the intermediate product undergoes mechanical stress or pressing at high temperature (typically 830–850 °C). Although the mentioned techniques allow one to obtain highly textured bulk samples demonstrating large values of critical current density, nevertheless these techniques are very laborious. In the present paper we suggest a new, easier method of preparation of textured Bi2223 and Bi2223/Ag ceramics which avoids pressing at high temperature.

The main idea of this method is to use foamed bulk Bi2223 superconductor [10, 11] having a flake-like microstructure as a precursor. This material consists of chaotically oriented plate-like crystallites which are joined via cleavage areas [11]. Uniaxial pressing of such a material may lead to an arrangement of crystallites so that the presence of micro-interstices in the precursor facilitates the turning of crystallites. Besides, the pressing of precursor was done in a liquid medium, so the hydrostatic stress drastically increases the ductility of a material [4].

2. Preparation and characterization of textured $Bi_{1.8}Pb_{0.3}Sr_{1.9}Ca_2Cu_3O_x$ and $Bi_{1.8}Pb_{0.3}Sr_{1.9}Ca_2Cu_3O_x$ + Ag superconductors

2.1. Preparation and characterization of precursors—foamed $Bi_{1.8}Pb_{0.3}Sr_{1.9}Ca_2Cu_3O_x$ and $Bi_{1.8}Pb_{0.3}Sr_{1.9}Ca_2Cu_3O_x$ + Ag superconductors

Preparation of foamed Bi2223-based samples was done in two steps [10, 11]. In the first stage initial powders Bi_2O_3, $SrCO_3$, PbO, CuO, and $CaCO_3$ taken in necessary proportions were ground, mixed thoroughly, pressed into pellets and then annealed at $T = 800$ °C for 24 h followed by regrinding and pressing into pellets. In the second stage pellets were annealed at $T = 820$ °C for 400 h.

Composite samples containing 20, 25, and 30 vol% of Ag were prepared in the same way. Ultra-dispersive Ag powder was added and mixed with the intermediate product after the

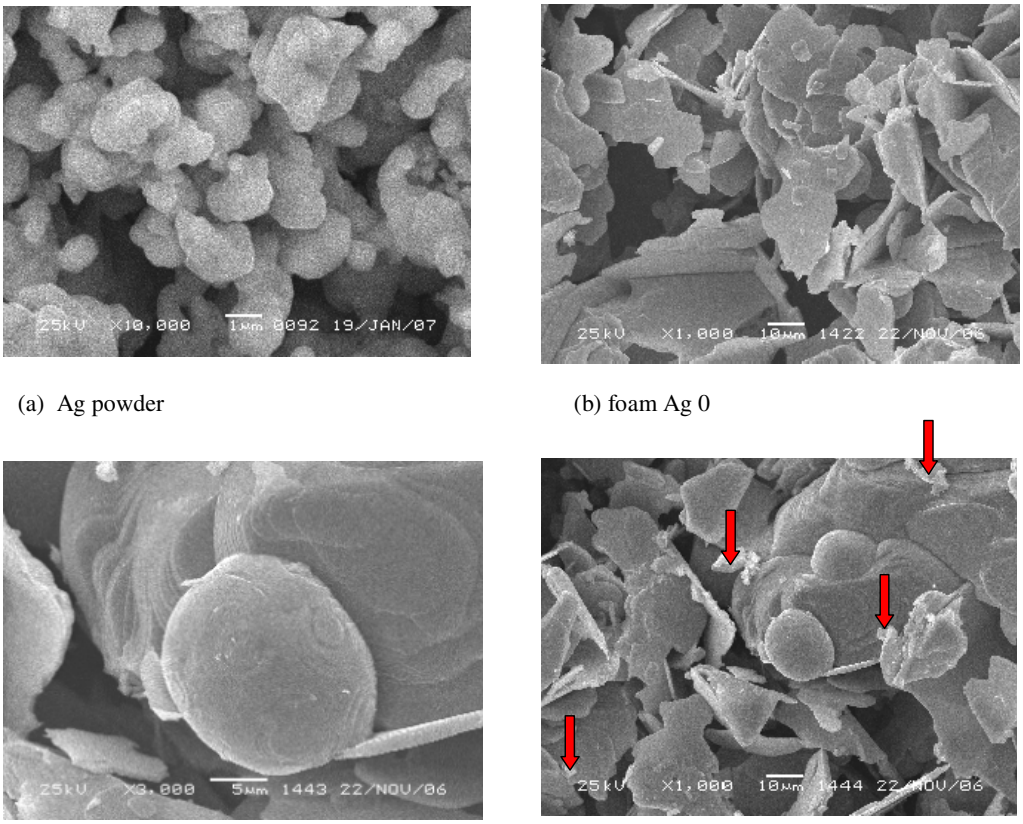

(a) Ag powder (b) foam Ag 0

(c) foam Ag 25 (d) foam Ag 25

Figure 1. SEM images of foamed Bi-based samples (precursors for textured ceramics) ((b), (d)) and of ultra-dispersive Ag powder (a) obtained using a commercial JEOL installation. In (b) a spherical Ag particle is shown. The arrows in (d) indicate Ag particles in foamed composite with 25 vol% of Ag.

first stage of preparation. The SEM image of ultra-dispersive Ag powder used is presented in figure 1(a). It is seen that this powder contains particles of $\sim$1 μm in diameter.

After annealing, the pellets increased in dimensions. The densities of materials obtained were 1.6 g cm^{-3} (26% of the theoretical one) for Bi-based foam and $\approx$1.2 g cm^{-3} (20% of the theoretical one) for Bi-based/Ag composites.

The x-ray analysis of foamed samples measured on a D8 ADVANCE (Brucker) powder diffractometer reveal that the structure 2223 is dominant; a small amount of Bi2212 phase (less than 5%) was also detected. Reflections from Ag are also seen on diffraction patterns of composites $Bi_{1.8}Pb_{0.3}Sr_{1.9}Ca_2Cu_3O_x$/Ag. Magnetic measurements have shown that all samples have critical temperature $T_C \approx 108$ K.

Typical scanning electron microscopy (SEM) images of foamed Bi-based samples are presented in figures 1(b) and (d). It is seen that the material has a pronounced flake-like microstructure. Crystallites of $Bi_{1.8}Pb_{0.3}Sr_{1.9}Ca_2Cu_3O_x$ have a form of plates of $\sim$1–2 μm in thickness and average linear dimensions $\sim$20–30 μm. The micro-interstices, having dimensions about $\sim$10–30 μm, are also clearly seen. Obviously, the crystallographic c-axes of $Bi_{1.8}Pb_{0.3}Sr_{1.9}Ca_2Cu_3O_x$ are perpendicular to the surface of plates and the a–b planes are parallel to the surface. We believe that during final heat treatment the crystallites grow predominantly in the a–b planes. Due to the random orientations of crystallites this growth led to the material volume increase [11].

Ag is seen on the SEM images of composites $Bi_{1.8}Pb_{0.3}Sr_{1.9}Ca_2Cu_3O_x$/Ag both as small ($\sim$1 μm, like that in the initial powder; see figure 1(a)) and sufficiently large spherical particles of 10–20 μm in diameter; see figures 1(c) and (d). During long time annealing at a temperature not far from the melting temperature of silver, a portion of $\sim$1 μm Ag particles of the ultra-dispersive silver powder seems to adhere and form spherical particles. Ag particles of both types are seen to be in close contact with crystallites of $Bi_{1.8}Pb_{0.3}Sr_{1.9}Ca_2Cu_3O_x$. The face-centered cubic lattice of silver becomes apparent on the surface of the spherical particles as fluted drawing containing hexagonal and rhombic traceries.

2.2. *Preparation of textured $Bi_{1.8}Pb_{0.3}Sr_{1.9}Ca_2Cu_3O_x$ and $Bi_{1.8}Pb_{0.3}Sr_{1.9}Ca_2Cu_3O_x$/Ag superconductors*

Foamed Bi-based samples were used as precursors for textured ceramics. The pellets of $\approx$4–4.5 mm height and $\approx$30 mm in diameter were impregnated by ethyl alcohol and then subjected to uniaxial pressing up to 200–500 MPa (along to the direction of symmetry axis of the pellet) at room temperature followed by drying at 70 °C for 5 h. The pressed pellets were annealed for 30–50 h at 830 °C. We found that after one circle of

Table 1. Designation and composition of textured samples.

Designation	Bi-HTSC vol. content (%)	Ag vol. content (%)	Bi-HTSC weight content (%)	Ag weight content (%)
Text Ag 0	100	0	100	0
Text Ag 20	80	20	69	31
Text Ag 25	75	25	63	37
Text Ag 30	70	30	57	43

'pressing in liquid medium → annealing' the samples obtained demonstrate a high degree of texture. The resulting materials had the form of pellets with typical dimensions ≈0.9–1.0 mm in height and ≈30 mm in diameter. The density of the materials obtained was ≈5.3 g cm^{-3} (≈ 90% of the theoretical one). The sample compositions (volume and weight contents) and designations are given in table 1.

In order to recognize the effect of texturing on the transport and magnetic properties a 'benchmark' polycrystalline sample was prepared. The foamed $Bi_{1.8}Pb_{0.3}Sr_{1.9}Ca_2Cu_3O_x$ ceramic sample was reground, pressed as a pellet and annealed at 830 °C for 25 h. The SEM image of the surface of this sample revealed a granular microstructure. The crystallites have the shape of plates but their average linear dimensions decreased down to ∼10 μm while the portion of small size crystallites (less than 10 μm) is increased in comparison with sample *text Ag 0*. No well pronounced texture was observed. Hereafter we denote this sample as *Bi-poly*. The density of the *Bi-poly* sample was ≈89% of the theoretical one.

2.3. X-ray analysis of textured samples

The x-ray diffraction patterns of textured samples are shown in figure 2. In the same way as for precursors (see above) the structure 2223 is dominant, and reflections from Ag are also seen on diffraction patterns of composite textured samples. The degree of orientation F was evaluated using the Lotgering method [12]:

$$P = \Sigma I(00l)/[\Sigma I(hkl)],$$

where $I(hkl)$ is the total intensity of (hkl) reflections, and $\Sigma I(00l)$ is the total intensity of $(00l)$ reflections. The F value is equal to 1.0 for ideally ordered crystallites. For quantitative analysis we took reflections from Bi2223 structure (002), (004), (008), (00$\underline{10}$), (00$\underline{14}$), (00$\underline{16}$), (00$\underline{20}$), and (115), (119), (11$\underline{15}$), (11$\underline{17}$), (11$\underline{19}$). The values of P are 0.97 ± 0.01 for sample *text Ag 0* and 0.98 ± 0.01 for composite samples with Ag manifesting the arrangement of the $Bi_{1.8}Pb_{0.3}Sr_2Ca_2Cu_3O_x$ crystallites in the materials obtained.

2.4. Microstructure of textured $Bi_{1.8}Pb_{0.3}Sr_{1.9}Ca_2Cu_3O_x$ and $Bi_{1.8}Pb_{0.3}Sr_{1.9}Ca_2Cu_3O_x$/Ag superconductors

Figure 3 shows typical SEM images of textured samples. The images from the surface of pellets (figures 3(a) and (b)) show that the Bi2223 crystallites have the form of plates similarly to the precursors used (figures 1(b) and (d)). The surfaces of the plates are in the plane of the face of the pellet.

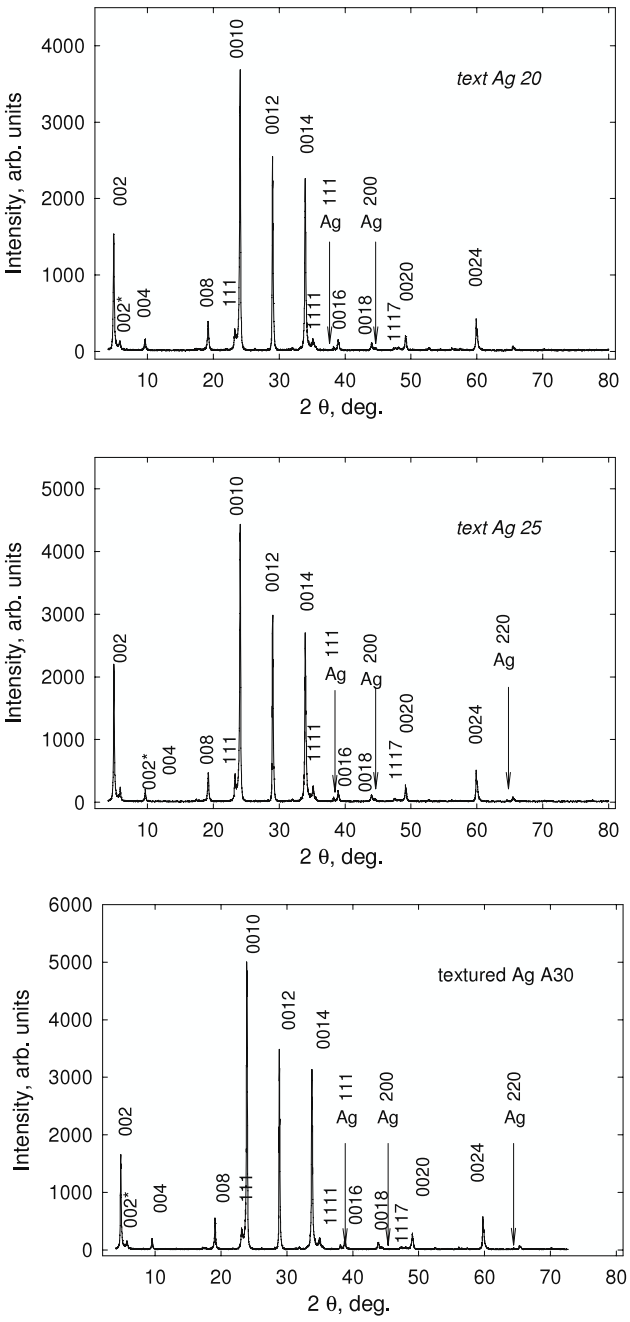

Figure 2. The x-ray diffraction patterns of textured composite samples.

The linear dimensions of the crystallites are nearly the same as those for the precursors (∼20–30 μm; see figures 1(b) and (d)). So, pressing of the precursor in the liquid medium facilitates turning of the crystallites and does not result in dramatic crushing of the crystallites. Note that Ag particles are also seen in the SEM images both as 'large' spheres (figure 3(a)) and small particles ∼1 μm in diameter. In order to observe texture in the direction of pressing, SEM images were obtained from different parts of natural chips of pellets; see figures 3(c) and (d). These images reveal that the plate-like $Bi_{1.8}Pb_{0.3}Sr_{1.9}Ca_2Cu_3O_x$ crystallites stand mainly perpendicular to the axis of pressing, i.e., parallel to the

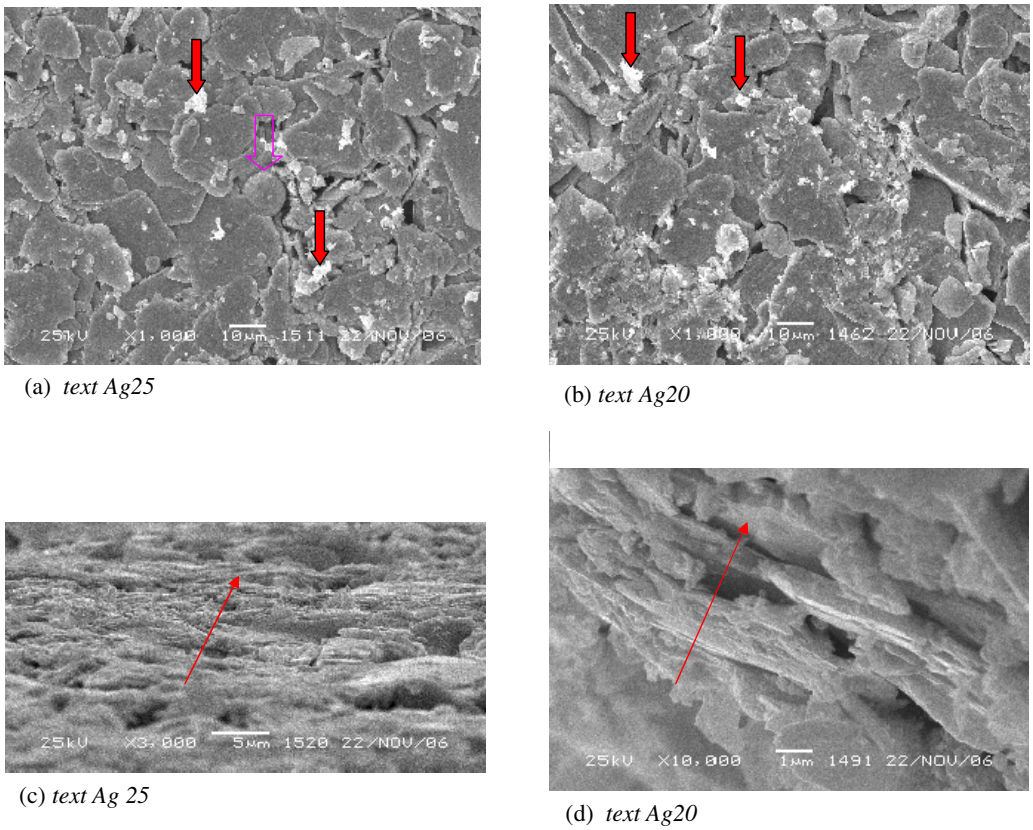

(a) *text Ag25* (b) *text Ag20*

(c) *text Ag 25* (d) *text Ag20*

Figure 3. Typical SEM images of textured samples obtained using commercial JEOL installation. ((a), (b))—the images from the surface of the pellets. Arrows in (a) and (b) indicate a spherical Ag particle (pink, open arrow) and small Ag particles (red, solid arrows). ((c), (d))—the images from natural chips of a pellet. Arrows in (c) and (d) indicate the direction of pressing ($\perp$ to the surface of pellet).

face of a pellet, and this ordering remains deep in the pellet. So, according to the images of microstructure, the materials obtained have pronounced texture: the *a*–*b* planes of plate-like $Bi_{1.8}Pb_{0.3}Sr_{1.9}Ca_2Cu_3O_x$ crystallites lie mainly parallel to the face of pellet while the *c*-axes are parallel to the pellet's axis of symmetry.

3. Experimental methods

Magnetic measurements were studied using a vibration sample magnetometer. A superconducting solenoid was used for generation of magnetic fields up to 60 kOe. For measurements of hysteretic loops of magnetization $M(H)$ at 77.4 K and temperature dependences of magnetization $M(T)$, a copper solenoid was used. For magnetic measurements, samples of cubic form $\sim 1 \times 1 \times 1$ mm^3 were cut from the pellets. The cubic samples of textured Bi2223 had the same symmetry as the pellets: two opposite facets correspond to the *a*–*b* planes of $Bi_{1.8}Pb_{0.3}Sr_{1.9}Ca_2Cu_3O_x$ crystallites. The $M(T)$ dependences were measured both in the zero field cooled (zfc) and field cooled (fc) regimes.

The transport properties (temperature dependences of resistance $\rho(T)$ and current–voltage characteristics (CVCs)) were measured by the standard four-probe technique under fixed DC current conditions. The sample was cut from a pellet in the form of a parallelepiped. The transport current direction was along to the *a*–*b* planes of $Bi_{1.8}Pb_{0.3}Sr_{1.9}Ca_2Cu_3O_x$ crystallites. The electrical contacts were made using epoxy Ag paste. For the CVC measurements the central part of the sample was polished down to thickness $\sim$0.2 mm. The CVCs were measured in a liquid nitrogen bath. The magnitude of transport critical current I_C was determined by the standard 1 μV cm^{-1} criterion.

4. Results and discussion

4.1. Magnetic properties

4.1.1. Temperature dependences of magnetization. Figure 4 shows the temperature dependences of magnetization $M(T)$ of textured ceramics for two different orientations ($\boldsymbol{H} \parallel c$-axis and $\boldsymbol{H} \parallel a$–$b$-planes) of samples measured at $H = 13$ Oe under zfc and fc conditions in comparison with the $M(T)$ dependences of a polycrystalline sample. The data in this figure and the following figures are presented in units 'emu per mass of the whole sample', i.e., this is the property of the composite material. The values of magnetization per mass of $Bi_{1.8}Pb_{0.3}Sr_{1.9}Ca_2Cu_3O_x$, i.e., the characteristic of superconductive phase in the composite, are given in table 2.

The critical temperature T_C is $\approx$108 K for all samples. The orientation magnetic anisotropy of textured samples is clearly seen from figures 4(a)–(d). The absolute values of

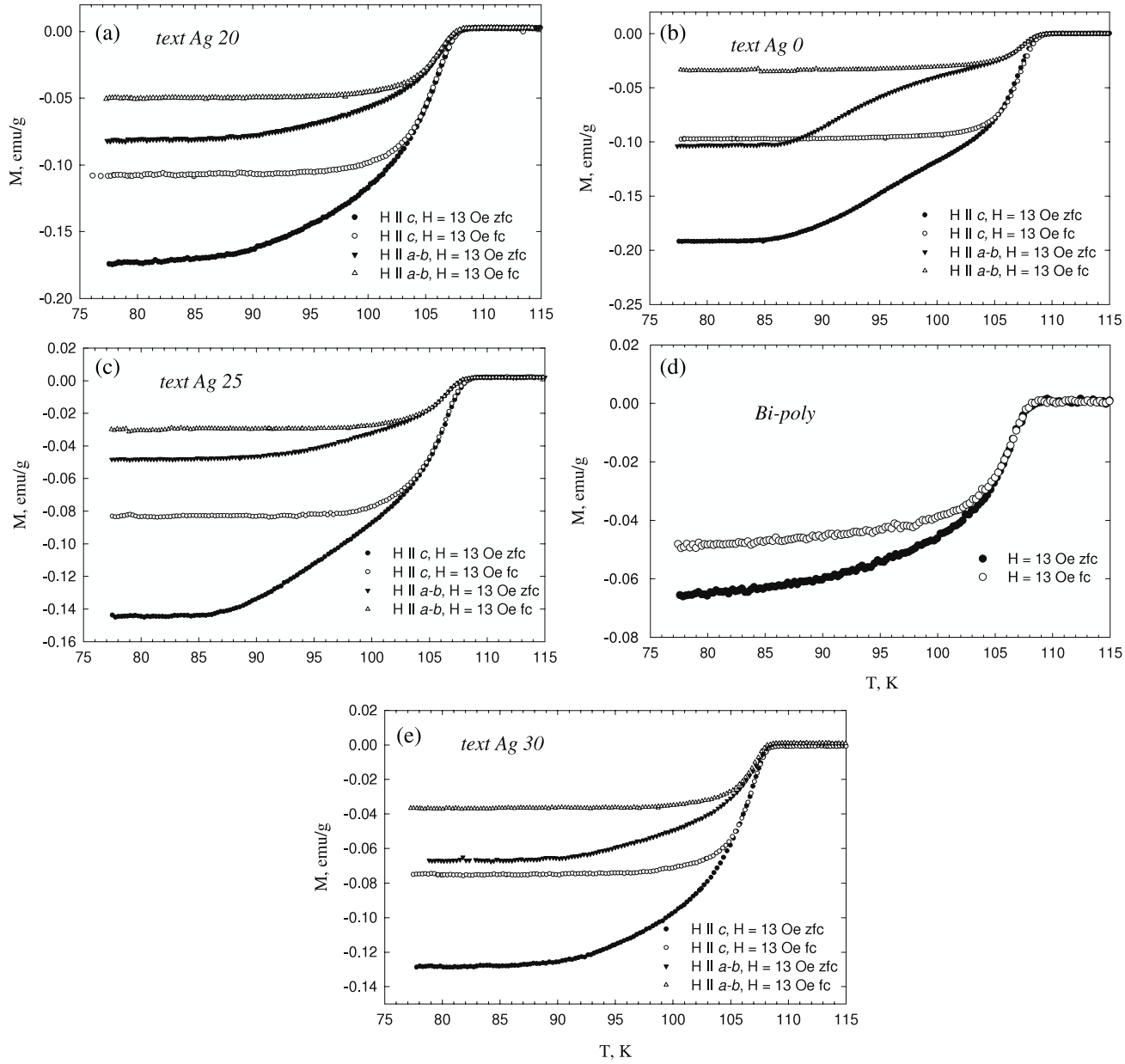

Figure 4. Temperature dependences of magnetization $M(T)$ of textured ceramics for two orientations ($H \parallel c$-axis and $H \parallel a$–b-planes) at $H = 13$ Oe under zfc and fc conditions and $M(T)$ of sample *Bi-poly*.

Table 2. The screening properties of textured samples. M_{zfc} and M_{fc} are magnetizations in emu per g of Bi2223 units at $H = 13$ Oe.

Sample	M_{zfc} (77.4 K) $\boldsymbol{H} \parallel c$ (emu/(g Bi2223))	M_{fc} (77.4 K) $\boldsymbol{H} \parallel c$ (emu/(g Bi2223))	M_{fc}–M_{zfc} (77.4 K) $\boldsymbol{H} \parallel c$ (emu/(g Bi2223))
Text Ag 0	−0.192	−0.0975	0.0945
Text Ag 20	−0.25	−0.156	0.094
Text Ag 25	−0.23	−0.132	0.098
Text Ag 30	−0.226	−0.132	0.094
Bi-poly	−0.066	−0.0475	0.018

magnetization are 2–3 times higher for the orientation $\boldsymbol{H} \parallel c$. Moreover, the difference M_{fc}–M_{zfc} is also 2–3 times higher for this orientation. Comparing $M(T)$ and M_{fc}–M_{zfc} data obtained on textured ceramics with those for the 'benchmark' *Bi-poly* sample (see figure 4(d)) one can see that the values of magnetization obtained on the composite textured ceramics for the orientation $\boldsymbol{H} \parallel c$ are significantly higher even without accounting the mass of Ag in the composites. On the other hand, the magnetization of the HTSC crystallites is practically the same for samples with various Ag content; see table 2.

Table 3. The magnitudes of remanent magnetization in emu per g of HTSC units of textured samples for various orientations of magnetic field and crystallographic axes of HTSC crystallites.

Sample	M_{rem} (77.4 K) $\boldsymbol{H} \parallel c$ (emu/(g Bi2223))	M_{rem} (4.2 K) $\boldsymbol{H} \parallel c$ (emu/(g Bi2223))	M_{rem} (4.2 K) $\boldsymbol{H} \parallel a$–$b$ (emu/(g Bi2223))
Text Ag 0	0.32	24.44	10.35
Text Ag 20	0.35	29.6	16.45
Text Ag 25	0.33	21.6	11.45
Text Ag 30	0.44	27.5	14.85
Bi-poly	0.1	10.0	

The magnitude of magnetization and the difference M_{fc}–M_{zfc} at sufficiently small external fields are known to be proportional both to pinning and screening currents [13]. So, the texture of micro-crystallites in bulk samples provides the magnetic anisotropy of the ceramic samples due to the anisotropy of the superconductive properties of Bi2223 crystallites.

It is worthwhile noting that the $M_{zfc}(T)$ dependences of sample *text Ag 0* exhibit a peculiarity—the change of curvature at $T \sim 88$ K ($\boldsymbol{H} \parallel a$–$b$) and $T \sim 93$ K ($\boldsymbol{H} \parallel c$). Such a peculiarity seems to arise from the effect of natural inter-crystallite boundaries so that the DC magnetization[4] at sufficiently small fields is determined by both inter-crystallite and intra-crystallite screening currents [13, 14]. This behavior correlates with transport critical current density data (the j_C (77.4 K) value for sample *text Ag 0* is noticeably less than for the composite samples; see section 4.2.2).

4.1.2. Hysteretic loops of magnetization and intra-crystallite critical currents. At intermediate ($\sim 10^2$–10^3 Oe) and high (10^4–10^5 Oe) external magnetic fields the intra-crystallite critical currents give the dominant contribution to the magnetization. The hysteretic loops of magnetization of textured samples at 77.4 K in the range of fields up to 1.6 kOe are presented in figure 5. These dependences also exhibit anisotropy with respect to the orientation. The magnetization in the direction $\boldsymbol{H} \parallel c$ is about two times higher than that for the $\boldsymbol{H} \parallel a$–$b$ direction. Since the specimens had cubic form, the effect of the shape demagnetization factor was the same for both $\boldsymbol{H} \parallel a$–$b$ and $\boldsymbol{H} \parallel c$ directions. Therefore, the magnetic anisotropy observed is due to the texture of the ceramic samples. Similarly to $M(T)$ data one can see that the magnetization of textured samples in the direction $\boldsymbol{H} \parallel c$ is higher than that for the 'benchmark' *Bi-poly* sample even in 'emu per g of sample' units. The values of remanent magnetization of Bi2223 phase in composite samples are given in table 3.

On the decreasing branches of the $M(H)$ curves the magnetization is negative in a wide field range, which points out that hysteretic $M(H)$ dependences are characteristic for geometric barrier or Bean–Livingston barrier [15, 16] models. Similar behavior was observed on textured and polycrystalline Bi2223 samples in the high temperature range [17, 18].

[4] The DC $M(T)$ dependence is proportional to susceptibility $\chi(T)$ ($\chi^2 = \chi'^2 + \chi''^2$) where χ' is determined by the effect of inter-grain boundaries; see for example [14].

Table 4. The intra-crystallite critical current densities at $T = 4.2$ K, $H = 0$ and the ratio J_C^{a-b}/J_C^c determined from $M(H)$ data of textured samples.

Sample	J_C^{a-b} (A cm^{-2})	J_C^c (A cm^{-2})	J_C^{a-b}/J_C^c
Text Ag 0	90×10^6	1.6×10^6	55
Text Ag 20	110×10^6	2.5×10^6	44
Text Ag 25	80×10^6	1.77×10^6	45
Text Ag 30	100×10^6	2.3×10^6	43

Figure 6 shows hysteretic loops of magnetization of textured samples at 4.2 K in the range of fields up to 60 kOe. The values of magnetization are increased up to ~30 times in comparison to M(77.4 K). This is in accordance with data for Bi2223 [17, 18]. The magnetic anisotropy of bulk textured samples is clearly seen in figure 6. The ratio $M(\boldsymbol{H} \parallel c)$ to $M(\boldsymbol{H} \parallel a$–$b)$ is ~2–2.5, and holds both for 77.4 and 4.2 K. In the low temperature range the shape of $M(H)$ curves is close to that predicted by the Bean model (ascending and descending branches have a plateau in the high field range and are nearly symmetrical).

One can estimate the value of intra-grain critical current density using the formula

$$J_C = 30 \times \Delta M/d,$$

derived from the Bean model [19, 20]. Here ΔM is the difference of positive and negative magnetizations in emu cm^{-3} units at a constant field and d is the average crystallite dimension for the case of polycrystalline superconductor [20]. For our textured samples d has the sense of crystallite dimension in the direction parallel to external field, so the critical current density is determined by the cross-section perpendicular to the circulating currents. If we take $\Delta M \approx 2M_{rem}$ (ΔM(emu cm^{-3}) = ΔM(emu g^{-1} of HTSC) $\times$ 5.95(g cm^{-3})), see table 3, $d \sim 1$ μm and $d \sim 25$ μm for the directions along the c-axis and in the a–b planes respectively, one obtain the values of J_C in the a–b planes (J_C^{a-b}) and along the c-axis (J_C^c) at zero external field. These data are presented in table 4. The magnitudes of intra-crystallite J_C^{a-b} at 4.2 K ($\sim 10^8$ A cm^{-2}) obtained are typical for Bi2223 superconductors. The anisotropy parameter J_C^{a-b}/J_C^c is about ~50 for all textured samples. This is in accordance with known data for Bi2223 [21]. This result additionally proves that the samples obtained in fact have a high degree of texture.

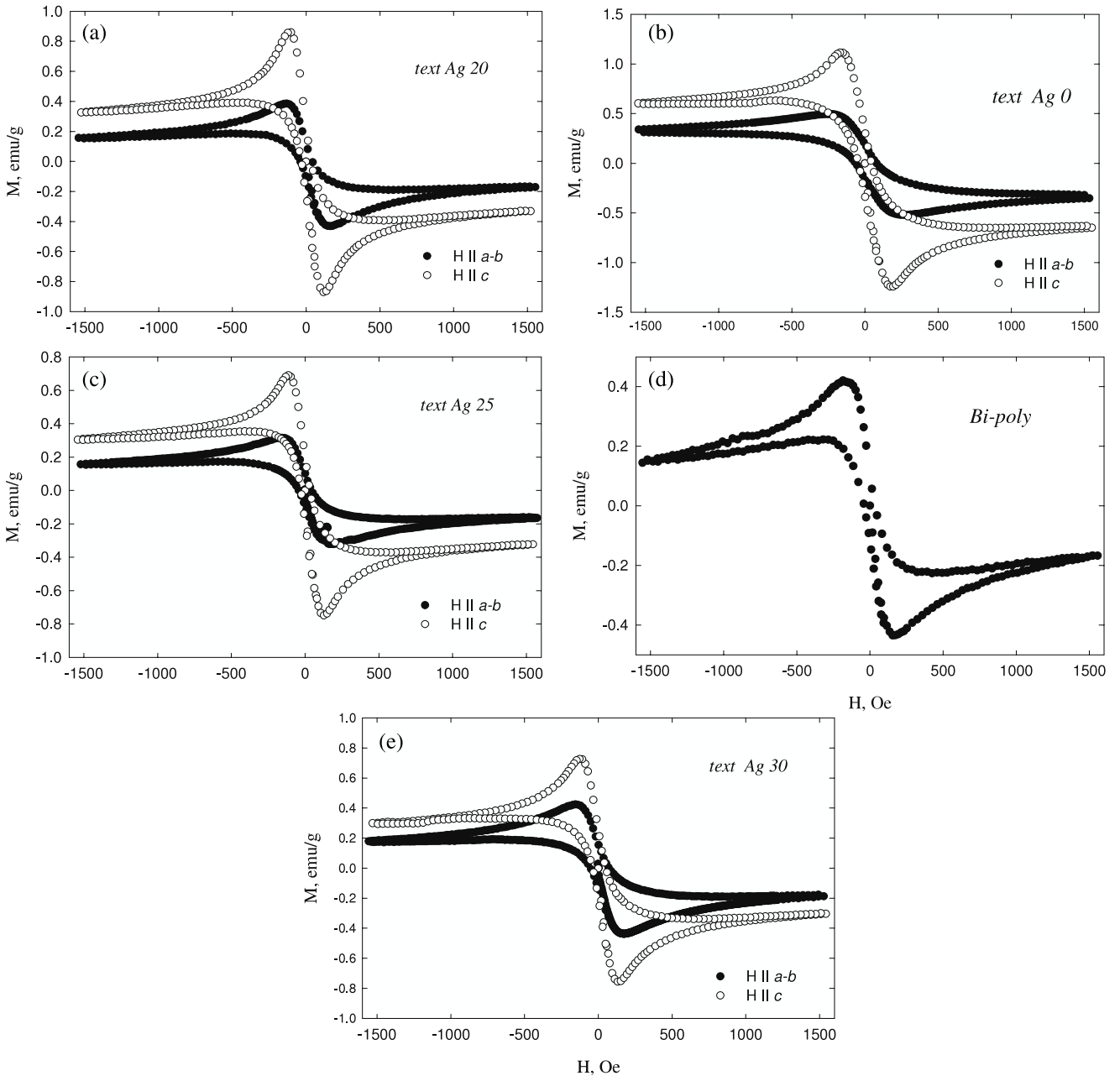

Figure 5. The hysteretic loops of magnetization $M(H)$ at 77.4 K of textured samples for two orientations ($H \parallel c$-axis and $H \parallel a$–b-planes) in the range of fields up to 1.6 kOe and $M(H)$ of sample *Bi-poly*.

4.2. Transport properties

4.2.1. Temperature dependences of resistivity. Figure 7 shows the temperature dependences of resistivity of textured samples and *poly-Bi* sample. The temperature of onset of the resistive transition is ∼113 K while T_C at $R = 0$ is ≈106 K for all samples. The absolute values of resistivity of textured samples with Ag additions are less than that for sample *text Ag 0*. We believe that this fact is due to the effect of silver particles which form inter-crystallite boundaries and improve the electrical contacts between Bi-2223 crystallites. Above ∼150 K the $\rho(T)$ dependences have metallic behavior. Extrapolation of the $\rho(T)$ dependences from the range $T > 150$ K to $T = 0$ gives the magnitude of residual resistivity. The behavior of this parameter versus the Ag content correlates with the dependence of normal state resistivity of samples on the Ag content. On the other hand, the resistivity of sample *text Ag 25* is somewhat less than that for sample *text Ag 25*. This fact correlates with data on transport critical currents; see section 4.2.2.

4.2.2. Transport critical current density. The transport critical current density j_C of polycrystalline HTSC first and foremost is determined by Josephson tunneling between superconducting crystallites. For this reason the j_C value is a characteristic of inter-crystallite boundaries. Figure 8

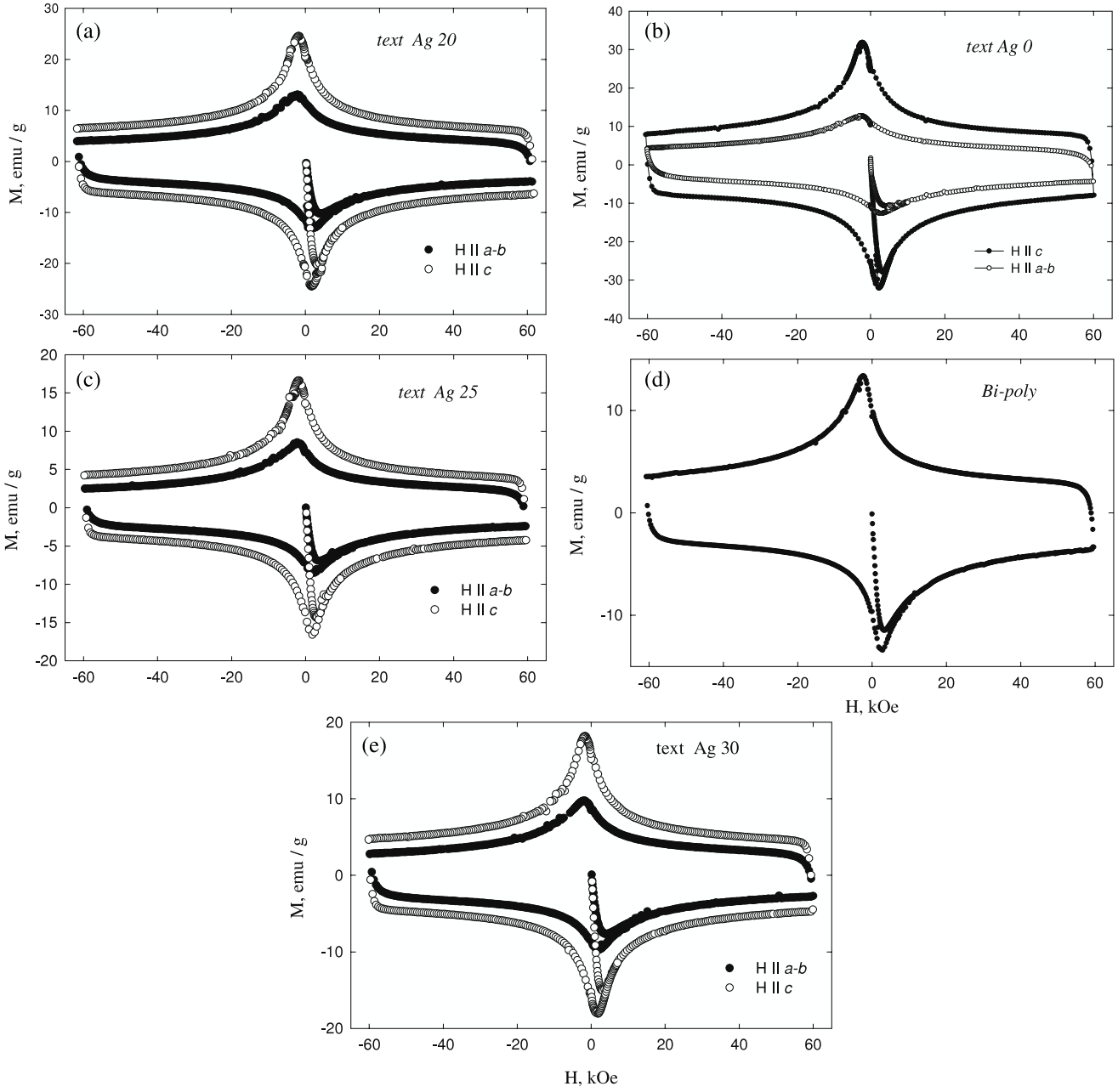

Figure 6. The hysteretic loops of magnetization $M(H)$ at 4.2 K of textured samples for two orientations ($H \parallel c$-axis and $H \parallel a$–b-planes) in the range of fields up to 60 kOe and $M(H)$ of sample *Bi-poly*.

shows CVCs at 77.4 K of the studied textured samples. The j_C(77.4 K) values are given in this figure. The textured sample without Ag addition has considerably lower j_C than those obtained on the composites. The $M(T)$ curves of sample *text* + *Ag 0*, measured at $H = 13$ Oe (in contrast to $M(T)$ of samples with Ag additions), demonstrate a peculiarity which reflects the poor quality of inter-crystallite boundaries; see figure 4 and section 4.1.1. Obviously, we are dealing with the well known fact that silver may improve the transparency of inter-crystallite boundaries for the supercurrent carriers [22]. We believe that the small Ag particles (1 μm or less) seen on SEM images of precursors and textured ceramics, see figures 1 and 3, provides better Josephson coupling than natural inter-crystallite boundaries. Spherical particles of 10–20 μm in diameter are too large to play the role of Josephson barriers between Bi2223 crystallites. The highest j_C value is obtained for the composite *text* + *Ag 25* and this sample has the lowest resistance in the normal state (see figure 7). At sufficiently large contents of Ag, it is more probable that ultra-dispersive particles seek to form large spherical particles and the effect of improvement of Josephson coupling becomes less pronounced. Apparently, the content of Ag 25 vol% is close to optimal to achieve the 'best' transparency of inter-crystallite boundaries. Note that value 25% is close to the percolation threshold of a three-dimensional two-phase system.

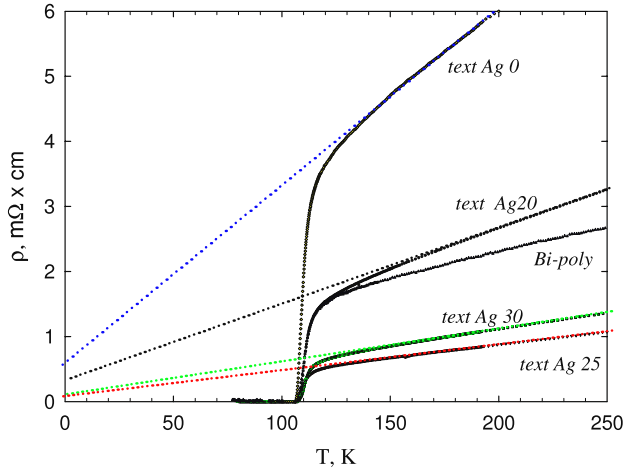

Figure 7. Temperature dependences of the resistance of textured samples and sample *Bi-poly*. Straight lines determine the residual resistivity (at $T = 0$).

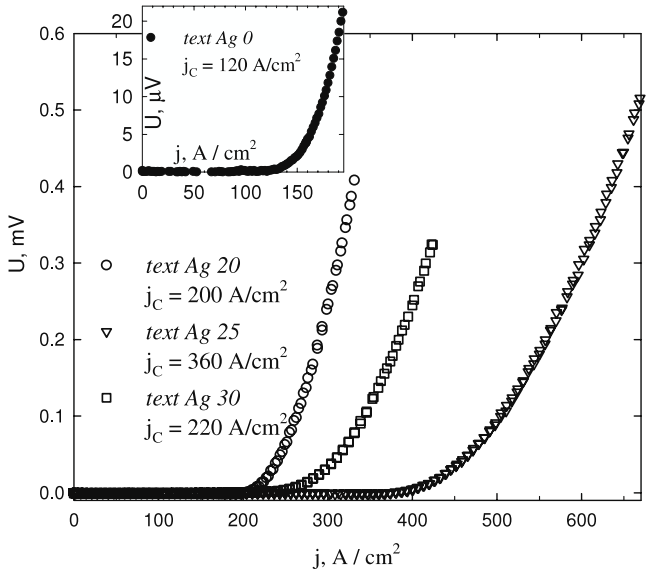

Figure 8. Initial portions of CVCs of textured composites and sample *text + Ag 0* (inset) at 77.4 K.

5. Concluding remarks

Thus, in this work a new method of preparation of bulk Bi2223 and Bi2223/Ag textured ceramics is proposed. In this method the porous superconducting materials having Bi2223 plate-like micro-crystallites of ∼1 μm in width and linear dimensions about 20–30 μm used as precursors were subjected to uniaxial pressing in liquid medium at room temperature followed by thermal treatment. The x-ray data analysis and SEM images of the samples obtained testifies that they have textured structure. The anisotropy of magnetization with respect to orientation of external magnetic field and crystallographic axes of micro-crystallites as well as estimation of the anisotropy parameter J_C^{a-b}/J_C^c additionally prove a high degree of texture in the samples obtained.

We believe that the following two factors mainly caused the texture formation in these materials. Firstly, the precursors used have flake-like microstructure in which the crystallites are sufficiently thin and have large enough linear dimensions. Secondly, the precursors were impregnated by liquid (ethyl alcohol), which penetrates into the micro-interstices. So, during pressing the crystallites are under conditions analogous to hydrostatic pressing. This provides a turning of Bi2223 crystallites without their being crushed.

Bulk textured composites Bi2223/Ag demonstrate large diamagnetic response in the direction perpendicular to orientation of *a–b* planes of Bi2223 crystallites both at 77.4 and 4.2 K, making these materials promising for possible practical applications in superconducting flywheels and magnets. Composites with 25 vol% of Ag addition demonstrate enhancement of transport critical current density at 77.4 K up to ∼360 A cm^{-2} due to the improvement of transparency of inter-crystallite boundaries by the effect of Ag.

Also, we note that the materials obtained are interesting for study of anisotropy of magnetic properties (magnetization hysteretic loops, melting point of Abrikosov vortex lattice, isothermal relaxation of magnetization, etc) of Bi2223 superconductors with respect to orientation of crystallographic axes of superconductive crystallites. This study is in progress at present.

Acknowledgments

This work is supported by program of RAS 'Quantum macrophysics' No. 3.4 and integration project of SB RAS No. 3.4 and in part by Krasnoyarsk Regional Scientific Foundation (KRSF), Grants 17G057, 18G148 and 18G011. DAB and AAD acknowledge the Russian Science Support Foundation.

References

[1] Wellhofer F *et al* 1990 *Supercond. Sci. Technol.* **3** 611
[2] Chen N *et al* 1993 *Supercond. Sci. Technol.* **6** 674–7
[3] Zhengping X and Lian Zh 1994 *Supercond. Sci. Technol.* **7** 908–12
[4] Desgardin G, Monot I and Raveau B 1999 *Supercond. Sci. Technol.* **12** R115–33
[5] Guilmeau E, Chateigner D and Noudem J G 2002 *Supercond. Sci. Technol.* **15** 1436–44
[6] Guilmeau E and Noudem J G 2002 *Supercond. Sci. Technol.* **15** 1566
[7] Li S, Bredehöft M and Gao W 1998 *Supercond. Sci. Technol.* **11** 1011–6
[8] Imayev M F *et al* 2007 *Physica* C **467** 14
[9] Grivel J-C 2007 *Supercond. Sci. Technol.* **20** 1059
[10] Petrov M I *et al* 2003 *Tech. Phys. Lett.* **29** 986
[11] Shaykhutdinov K A *et al* 2007 *Supercond. Sci. Technol.* **20** 491–4
[12] Lotgering F K 1959 *J. Inorg. Nucl. Chem.* **9** 113–9
[13] Malozemoff A 1989 *Physical Properties of High Temperature Superconductors* ed D M Ginsberg (Singapore: World Scientific)
[14] Berling D, Loegel D, Mehdaoui A, Regnier S, Caranoni C and Marfaing J 1998 *Supercond. Sci. Technol.* **11** 1292–9
[15] Fistul M *et al* 1995 *Phys. Rev.* B **52** R739
[16] Pissas M and Stamopoulos D 2001 *Phys. Rev.* B **64** 134510

[17] Kimishima Y, Ichikawa H, Takano S and Kuramoto T 2004 *Supercond. Sci. Technol.* **17** S36
[18] Lelovic M, Krishnaraj P, Erort N G and Balachandran U 1995 *Supercond. Sci. Technol.* **8** 336
[19] Bean C P 1962 *Phys. Rev. Lett.* **8** 250
[20] Chen D-X, Gross R W and Sanchez A 1993 *Cryogenics* **33** 695–702
[21] Grasso G *et al* 1999 *Supercond. Sci. Technol.* **12** 1108–11
[22] Su X, Giannini E and Flükiger R 2005 *Supercond. Sci. Technol.* **18** 830